Title

LIF signaling regulates outer radial glial to interneuron fate during human cortical development

Journal

Cell Stem Cell, 30(10)

ISSN

1934-5909

Authors

Andrews, Madeline G
Siebert, Clara
Wang, Li
et al.

Publication Date

2023-10-01

DOI

10.1016/j.stem.2023.08.009

HHS Public Access

Author manuscript

Cell Stem Cell. Author manuscript; available in PMC 2023 October 23.

Published in final edited form as:

Cell Stem Cell. 2023 October 05; 30(10): 1382–1391.e5. doi:10.1016/j.stem.2023.08.009.

LIF signaling regulates outer radial glial to interneuron fate during human cortical development

Madeline G. Andrews[1,2,3,8,*], **Clara Siebert**[1,2,8], **Li Wang**[1,2,8], **Matthew L. White**[1,2], **Jayden Ross**[1,2], **Raul Morales**[1,2], **Megan Donnay**[3], **Gradi Bamfonga**[3], **Tanzila Mukhtar**[1,2], **Arpana Arjun McKinney**[2,4,7], **Kaila Gemenes**[1,2,3], **Shaohui Wang**[1,2], **Qiuli Bi**[1,2], **Elizabeth E. Crouch**[2,5], **Neelroop Parikshak**[1,2], **Georgia Panagiotakos**[2,4,7], **Eric Huang**[1,2], **Aparna Bhaduri**[1,2,6], **Arnold R. Kriegstein**[1,2,9,*]

[1]Department of Neurology, University of California, San Francisco (UCSF), San Francisco, CA 94143, USA

[2]The Eli and Edythe Broad Center of Regeneration Medicine and Stem Cell Research, UCSF, San Francisco, CA 94143, USA

[3]School of Biological and Health Systems Engineering, Arizona State University (ASU), Tempe, AZ 85281, USA

[4]Department of Biochemistry and Biophysics, UCSF, San Francisco, CA 94143, USA

[5]Department of Pediatrics, UCSF, San Francisco, CA 94143, USA

[6]Department of Biological Chemistry, University of California, Los Angeles (UCLA), Los Angeles, CA 90095, USA

[7]Departments of Psychiatry and Neuroscience, Black Family Stem Cell Institute, Seaver Autism Center for Research and Treatment, Alper Center for Neural Development and Regeneration, Friedman Brain Institute, Icahn School of Medicine at Mount Sinai, New York, NY, 10029, USA

[8]These authors contributed equally

[9]Lead contact

SUMMARY

Radial glial (RG) development is essential for cerebral cortex growth and organization. In humans, the outer radial glia (oRG) subtype is expanded and gives rise to diverse neurons and glia. However, the mechanisms regulating oRG differentiation are unclear. oRG cells express leukemia-

*Correspondence: madeline.andrews@asu.edu (M.G.A.), arnold.kriegstein@ucsf.edu (A.R.K.).

AUTHOR CONTRIBUTIONS

Conceptualization, M.G.A. and A.R.K.; methodology, M.G.A., C.S., L.W., and A.B.; investigation, M.G.A., C.S., L.W., M.L.W., J.R., R.M., M.D., G.B., T.M. A.A.M., K.G., S.W., Q.B., N.P., and E.E.C.; formal analysis, L.W., A.B., M.G.A., C.S., M.L.W., and G.B.; writing – original draft, M.G.A. and C.S.; writing – review & editing, M.G.A., C.S., L.W., G.P., and A.R.K.; funding acquisition, M.G.A. and A.R.K.; resources, A.R.K., M.G.A., E.E.C., and E.H.; supervision, M.G.A., E.H., G.P., A.B., and A.R.K.

SUPPLEMENTAL INFORMATION

Supplemental information can be found online at https://doi.org/10.1016/j.stem.2023.08.009.

DECLARATION OF INTERESTS

A.R.K. is a co-founder, consultant, and member of the Board of Neurona Therapeutics.

inhibitory factor (LIF) receptors during neurogenesis, and consistent with a role in stem cell self-renewal, LIF perturbation impacts oRG proliferation in cortical tissue and organoids. Surprisingly, LIF treatment also increases the production of inhibitory interneurons (INs) in cortical cultures. Comparative transcriptomic analysis identifies that the enhanced IN population resembles INs produced in the caudal ganglionic eminence. To evaluate whether INs could arise from oRGs, we isolated primary oRG cells and cultured them with LIF. We observed the production of INs from oRG cells and an increase in IN abundance following LIF treatment. Our observations suggest that LIF signaling regulates the capacity of oRG cells to generate INs.

In brief

Andrews, Kriegstein, and colleagues observed that LIF signaling regulates outer radial glia (oRG) stem cells in developing human cerebral cortex tissue and forebrain organoids. They find that LIF shifts oRG production toward inhibitory interneurons that resemble cells derived from the caudal ganglionic eminence, with implications for excitatory/inhibitory balance.

Graphical Abstract

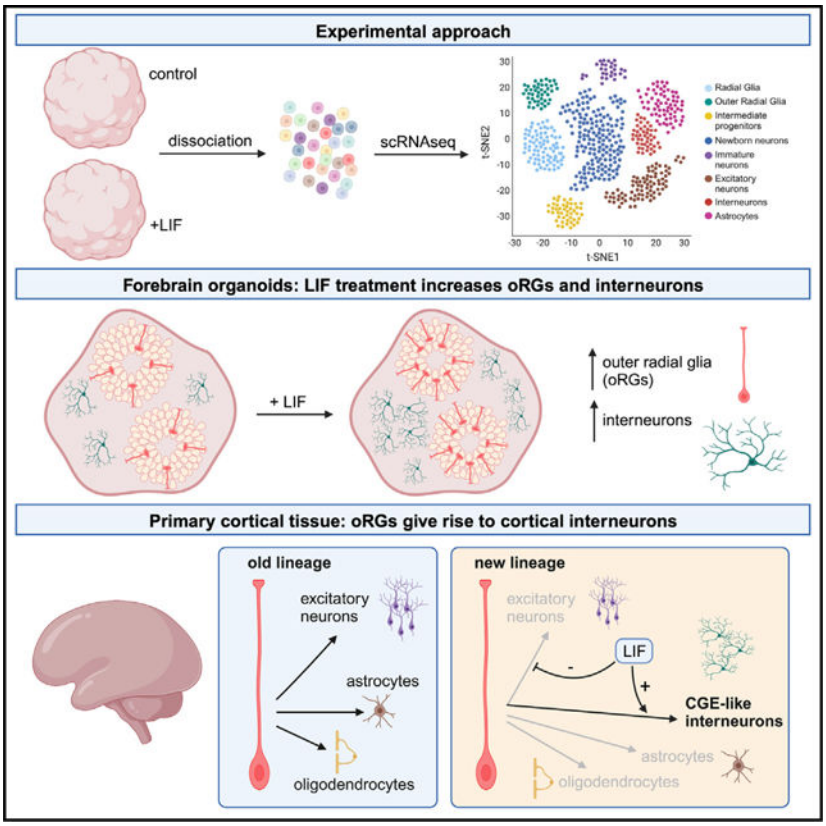

INTRODUCTION

The increased cellular diversity of the human cerebral cortex, compared with other species, presents compounding challenges for disentangling how developmental mechanisms impact mature neurological function. Recent studies of human neurogenesis have provided insights

into the molecular signatures of neural stem cells and their neuronal and glial progeny.[1–6] However, the local cues in the cortical niche that dictate fate decisions have not been explored in depth.

The human cerebral cortex contains cortical stem cells known as outer (oRG) or basal radial glia. These cells are positioned in an expanded progenitor domain, the outer subventricular zone (oSVZ), and are hypothesized to preferentially contribute to the generation of upper cortical layer neurons, which are expanded in humans.[7–10] However, the signaling mechanisms that regulate oRG fate determination have not been fully explored. Previous studies indicate that the leukemia-inhibitory factor (LIF) receptor (LIFR) is more highly expressed by oRG cells than other cortical cell types,[11] suggesting that LIF signaling may selectively influence oRG development. LIF signals through a heterodimeric complex of LIFR and gp130 that phosphorylates the intracellular proteins, JAK and STAT3,[12,13] to target regulatory pathways and initiate transcription. Increasing LIF levels in rodent embryos promotes cortical progenitor proliferation.[14,15] *In vitro* studies of rodent neurodevelopment also suggest that LIF supports the maintenance of radial glia (RG)-like cells.[16] Recent studies using human regionalized forebrain organoids observed that LIF was sufficient to increase the size of the oRG domain[17] and the production of astrocytes,[18] suggesting that LIF signaling may regulate oRG self-renewal and fate determination.

We sought to address the role of LIF signaling in oRG proliferation and differentiation using *in vitro* models of human development, pluripotent stem cell (PSC)-derived regionalized forebrain organoids, and primary cortical tissue. We found that activating LIF signaling promoted proliferation and increased the number of oRG cells in both organoids and primary cortical tissue. Surprisingly, we also observed an increase in inhibitory interneurons (INs) upon LIF treatment. To determine the potential source of these INs, we purified oRG cells from primary human cortical tissue and allowed spontaneous differentiation. We found that oRG cells differentiated into excitatory neurons (ENs), glial cells, and INs, and treatment with LIF increased IN production, suggesting that LIF signaling can promote the differentiation of INs from oRGs. Thus, changes in cortical fate determination regulated by LIF signaling may fine-tune the neuronal composition of the developing cortex.

RESULTS

Spatial patterns of LIF and LIFR in the developing human telencephalon

To determine the cell types in which LIF signaling is active in the developing telencephalon, we performed immunolabeling of LIFR in combination with NESTIN to label RG in the human dorsal cortex and ganglionic eminence (GE) (Figure 1A). We observed significant LIFR abundance in dorsal cortical RG but absence in ventral GE cells. We then evaluated LIF protein in the dorsal and ventral cortex and observed a significant overlap of LIF with DCX+ newborn neurons only in the dorsal telencephalon. Additionally, we analyzed single-cell RNA sequencing (scRNA-seq) datasets[2] to evaluate *LIFR* expression across multiple neural regions. We observed the highest *LIFR* expression in the neocortex and minimal expression in the GE or other ventral structures (Figure 1B).

We performed immunostaining for LIF signaling mediators in primary cortical tissue during peak neurogenesis from gestational weeks (GWs) 13–19. We observed that LIFR-expressing cells in the oSVZ were co-labeled with the oRG marker, HOPX, confirming the enrichment of LIFR in oRGs[11] (Figure 1C). This is consistent with reanalysis of published primary cortical tissue[19] and organoid scRNA-seq datasets[20] (Figures S1A and S1B). We observed LIF accumulation in the cortical plate, where ENs reside, suggesting that they may be a source of secreted LIF protein (Figures 1D, S1C, and S1D). Further supporting this hypothesis, we found a significant overlap between cortical ENs immunostained with the pan-neuronal marker NEUN and LIF. There is also significant co-expression of LIF with neuronal markers across development; first, early in neurogenesis, with the deep layer neuron marker, CTIP2/BCL11B, and later, with the upper-layer neuron marker, SATB2 (Figures 1D, right and S1D). Throughout peak neurogenesis, LIF protein appears most abundant in the cortical plate, where the basal processes of radial glia transit. LIF signaling may be activated in oRG cells through their basal processes which express LIFR (Figures S1E–S1H). These results, and previous studies,[11,17] suggest that secreted LIF is present during peak neurogenesis, and cortical oRG cells are likely to be a major cell type responsive to LIF signaling.

Perturbation of LIF signaling in cortical tissue impacts progenitor proportions

To determine the function of LIF signaling in cortical development, we performed pharmacological manipulations in organotypic slice cultures of primary cortical tissue (Figure 1E). Cultures were treated with either recombinant LIF protein to activate LIF signaling or SC144[21,22] or ruxolitinib[23,24] to inhibit the LIF signaling effectors, gp130 and JAK1/2, respectively (Figure S1I). LIF inhibition significantly decreased the number of HOPX+ oRG cells after 1 week in culture. In contrast, LIF activation significantly decreased the number of EOMES+ intermediate progenitor cells of the EN lineage (IPC_EN) (Figure 1F). Thus, activation of LIF signaling appears to increase the number of oRG cells and inhibition of LIF promotes their differentiation into excitatory neurogenic IPC_EN.

Under these experimental conditions, we did not observe a significant change in the numbers of dividing RG or postmitotic ENs (Figures S1J and S1K). However, organotypic culture viability limited the duration of treatment, and endogenous LIF within cortical tissue may limit the capacity to observe an increase with exogenous LIF. We turned to human PSC-derived regionalized dorsal forebrain organoids as an orthogonal approach to examine the impact of LIF on oRG cells.

LIF signaling promotes oRG expansion

To determine how LIF impacts oRG proliferation, we added LIF during peak oRG expansion (6–8 weeks) in this cortical organoid model[20,25] (Figure 2A). Immunofluorescence staining indicated that LIF treatment increased the number of HOPX+/GFAP+ oRG-like cells in the organoids by week 10 (Figure 2B). However, there was no observed impact on the expansion of the oRG population after extending the culture to 15 or 24 weeks (Figure 2B). Continuous LIF exposure from week 5 onward led to oRG proliferation up to week 15 (Figure 2C), as indicated by an increase in the number of

HOPX+/GFAP+/SOX2+/pHH3+ dividing oRG cells. Together, these data suggest that LIF signaling promotes oRG expansion.

To determine the impact of LIF signaling on oRG differentiation, we added LIF to forebrain organoids between weeks 6 and 8 and collected organoids at weeks 8, 10, and 15 for scRNA-seq (Figures 2D and S2). Organoid-derived cells expressed the forebrain marker, *FOXG1*, and included the expected diversity of cortical cell types, including *SOX2*+/*GFAP*+/*HOPX*+RGs, *EOMES*+IPC_ENs, and *NEUROD6*+ Ens (Figure 2E). Consistent with our immunohistochemistry data, quantification of cell populations captured by scRNA-seq revealed a small increase in the proportion of dividing RG cells at weeks 8 and 10 upon LIF treatment (Figure 3B).

LIF signaling promotes IN production

Previous studies of regionalized dorsal forebrain organoids have consistently demonstrated the emergence of INs, typically born at later time points.[26,27] We also identified several IN lineage markers in our scRNA-seq dataset, including *GAD1*, *GAD2*, *DLX1*, *DLX5*, *ASCL1*, and *BEST3*. Since *ASCL1* and *BEST3* are preferentially expressed in IN progenitors in the ventral telencephalon[19,28] (Figure 3A), we defined *GAD2*+/*DLX5*+/*ASCL1*+/*BEST3*+IN progenitors as IPCs for INs (IPC_IN) and *GAD2*+/*DLX5*+/*BEST3*− cells as INs. Surprisingly, we observed a significant increase in the proportion of IPC_INs and INs in our organoids following LIF exposure (Figure 3B). We performed differential expression analysis and observed a significant increase in several IN markers, including *DLX1*, *DLX5*, and *GAD2*, after LIF treatment (Figure 3C). To validate these findings, we performed immunostaining for IN markers and observed an increase in the number of DLX5+ and GABA+ cells in LIF-treated organoids (Figure 3D). As organoids could potentially have mixed regional identities, we complemented this analysis using primary cortical tissue samples. After treating organotypic slice cultures with LIF for 1 week, we observed an increase in the number of DLX5+ cells (Figure 3E), suggesting that LIF treatment may increase INs in isolated dorsal cortical tissue.

Although we found a proportional decrease of IPC_ENs and ENs in our scRNA-seq data (Figure 3B), no change in the absolute numbers of these populations was observed by immunohistochemistry (Figure S2D). However, after continuous LIF exposure from week 5 onward, there was a significant reduction in EOMES+ IPC_ENs and NEUN+/SATB2+ upper-layer ENs in cortical organoids, reflected by both scRNA-seq and immunostaining (Figure S3). Thus, LIF treatment increased the number of INs with a concomitant decrease in excitatory neurogenesis. Additionally, when we inhibited LIFR signaling in organoids with the gp130 inhibitor, SC144 beginning at week 5 of differentiation, we observed a decrease in the number of DLX5+ IN (Figure S2F). Together, these data suggest that LIF signaling is a regulator of DLX5+ IN production.

CGE-like INs generated in dorsal forebrain organoids

A recent lineage tracing study found that dorsal forebrain progenitors can give rise to both excitatory and inhibitory neurons,[29] with most INs in the study resembling cells derived from the caudal GE (CGE) (Figure S4). We wondered if the same cellular trajectories could

be recapitulated in dorsal forebrain organoids. We performed an unbiased characterization of IN cell types in dorsal forebrain organoids by comparing our organoid datasets to primary human GE-derived INs.[4] We assigned CGE, lateral GE (LGE), or medial GE (MGE) identities to individual IN clusters in our organoid data based on correlation to the corresponding IN subtypes from human ventral telencephalon (Figure S5A; STAR Methods). We observed that LGE-like INs were present at 8 weeks in organoids but were gradually replaced by CGE-like INs over time (Figure 4A). By 15 weeks, the majority of INs in organoids were CGE-like.

To better understand the IN subtypes present in organoids, we annotated the primary GE dataset at a more granular level (Figure S5B). We found that CGE-like neurons mostly resembled two IN subtypes: NR2F2+/PROX1+ INs found in CGE and MEIS2+/PAX6+ INs found in both CGE and LGE (Figures S5C and S5D). Based on transcriptional correspondence to primary primate IN subtypes, these CGE-like INs were projected to become cortical INs, olfactory bulb INs, deep white matter interstitial neurons, or eccentric spiny projection neurons[31] (Figure S5E). This observation was further confirmed using mutual nearest neighbor-based label transfer to determine IN subtypes (Figures S6A–S6C). Together, these results indicate that CGE-like INs can be generated by cortical progenitors in dorsal forebrain organoids similar to the developing human neocortex.

To determine if the identified IN trajectories in our dataset can be generalized, we examined the identity of INs in published dorsal forebrain organoid datasets.[30] We found that organoids cultured for relatively short durations (28 days) contained INs without clear identity (Figure S6D). However, CGE-like INs arose progressively over 3–6 months of differentiation (Figures 4B and 4C). Mutual nearest neighbor-based label transfer led to similar conclusions (Figure S6). Thus, the late generation of CGE-like INs is a reproducible phenomenon of human dorsal forebrain organoids.

LIF signaling increases CGE-like INs in organoids

We next asked which IN types were increased in dorsal forebrain organoids after LIF exposure. We performed differential expression analysis and established module eigengenes (STAR Methods) for genes expressed in CGE, LGE, or MGE. We observed significantly increased expression of CGE genes after LIF treatment (Figure S7A). LGE genes were also modestly increased, whereas MGE genes were absent in both control and LIF-treated organoids (Figures S7B and S7C). The correlation-based comparative analysis demonstrated that LIF treatment between weeks 6 and 8 increased both newborn and CGE-like INs. We observed a particular increase in CGE INs at week 10, when upper-layer excitatory neurogenesis typically occurs in our forebrain organoid protocol[20,25] (Figure 4D). Similar results were obtained by the label transfer method or the more granular IN subtype annotation (Figures S6A and S6B). To validate these findings, we probed CGE marker expression using fluorescent *in situ* hybridization in primary organotypic cortical cultures that were exposed to LIF for 1 week. Primary tissue had increased CGE maker gene expression, including *PCDH9* and *SCGN*, in the oSVZ where the oRG cells reside (Figures 4E, S7D, and S7E). Furthermore, immunostaining of organoids treated with LIF also indicated an increased proportion of cells expressing the CGE markers, SCGN and NR2F1

(Figure S7F). These results support our findings that LIF promotes the local production of CGE-like INs in human dorsal forebrain.

LIF exposure increases IN generation from isolated oRG cells

Increased CGE-like IN generation after LIF exposure in the oSVZ of cortical slices and during oRG expansion in organoids suggests that oRG cells may give rise to the CGE-like INs. To test this hypothesis, we isolated LIFR+ oRG cells from primary cortical tissue samples by fluorescence-activated cell sorting (FACS) (Figure S8A). We validated oRG enrichment using scRNA-seq and immunostaining, which indicated sorted cells express *SOX2*, *HOPX*, GFAP, *LIFR*, and *VIM* (Figures S8B–S8D). We cultured isolated oRGs in the presence of LIF for 1 week and allowed them to differentiate for an additional 3 weeks. We observed that oRG cells produced both ENs and INs, as well as glial cells, including astrocytes and oligodendrocyte precursor cells (OPCs) (Figures 4F and S8B–S8F). To exclude the possibility that INs derived from sorted oRGs were due to contamination from IN precursors, we sorted individual oRG cells into single wells in 96-well plates. After 4 weeks, we observed individual wells containing cells of both excitatory and inhibitory lineages (Figure S8G), further confirming that INs can be derived from oRGs.

oRG-derived IPC_INs robustly expressed *DLX5* and *BEST3* and the differentiated INs expressed *DLX5*, whereas MGE markers, *LHX6* or *NKX2–1*, were not expressed (Figure 4G). We observed robust expression of CGE markers, such as *SCGN*, *PROX1*, and *SP8*, and increased proportions of INs corresponding to those of CGE origin (Figures 4H, 4I, and S8H). Immunohistochemistry further validated a significant increase in DLX5+ INs after LIF treatment (Figure 4J). Our findings suggest that oRG cells can differentiate into locally derived CGE-like forebrain INs and that LIF signaling promotes this process.

DISCUSSION

Our findings underscore how early developmental signaling regulates cortical patterning and impacts the relative abundance of neuronal populations. We highlight a cytokine, LIF, that drives expansion of a key cortical stem cell population, oRG cells, in the human brain. Surprisingly, we also found that LIF exposure promotes IN production from oRG cells.

INs derived from the CGE contribute to ~30% of cortical INs in the mouse and typically reside in the upper cortical layers,[32,33] whereas ~70% of INs come from the MGE. Different proportions of IN subtypes are present across human cortical areas, with greater numbers of INs compared with mouse.[4,34–36] In disorders where the ventral telencephalon does not develop properly, MGE-derived IN types are absent, but CGE-like INs are still present, suggesting that a subset of CGE-like cells may be derived from another tissue source.[37] Our results suggest that cortical oRG cells are an additional source of INs in developing cortex.

Many studies have now demonstrated dorsal lineage restriction in regionalized forebrain organoids and reproducible cortical cellular diversity, validating the robustness of regionalized organoid protocols.[27,30,38] However, the predominant INs in forebrain organoids appear to be CGE-like, whereas most cortical INs arise from the MGE.[39] Thus, INs generated by dorsal forebrain organoids do not reflect the predominant cortical IN

subtypes, a feature that should be taken into account when using organoids to study cortical circuits or diseases with disrupted IN development. Assembloid models, in which independently regionalized dorsal and ventral forebrain organoids are fused, may better replicate cortical IN subtype diversity.[40–43]

The expansion of presumptive oRG-derived INs with CGE-like gene expression in our LIF-treated organoids speaks to a previously unknown regulator of human cortical fate determination. There are several potential sources of the LIF signal. Although LIF accumulates in cortical plate neurons, it is unknown whether the neurons produce LIF or whether LIF is derived from neighboring cell types, such as the innervating vasculature. Given the immunomodulatory function of LIF in injury and its role in regulating both vascular and immune development,[12,44–46] it may derive from a variety of non-neural cell types. Future studies should work to identify the cellular source of LIF secretion.

Finally, the downstream consequences of LIF-mediated local IN production, as well as implications for neurological disorders, are unclear. Human patients with alterations in LIF signaling suffer severe neurodevelopmental consequences as well as impaired development of other tissues, leading to shortened life expectancy.[47,48] More subtle alterations in LIF signaling, perhaps due to inflammation or injury, will be important to explore to determine the range of impacts LIF can have during cortical development. Future studies investigating the long-term effects of altered LIF signaling will be important to understand the regulation of EN and IN proportions, cortical organization, and circuit function, as well as the onset of disorders associated with altered neuronal excitability, such as epilepsy.

Limitations of the study

This study provides evidence of an oRG-derived IN population. However, there are technical limitations that limit the scope of our conclusions. Although we used multiple PSC lines and primary cortical tissue samples, experiments on human cells are limited in their capacity to encompass human genetic and biological variability. We found that oRG-derived INs are CGE-like, but their gene expression profiles reflect early-stage neurons, thus their final transcriptional and functional identity may be slightly different. Another limitation of this study is that experimental manipulations were performed *in vitro*, as molecular tracing of *in vivo* human brain development is not feasible.

STAR★METHODS

RESOURCE AVAILABILITY

Lead contact—Further information and requests for resources and reagents should be directed to and will be fulfilled by the lead contact, Arnold Kriegstein: Arnold.Kriegstein@ucsf.edu.

Materials availability—This study did not generate new unique reagents.

Data and code availability—Organoid data has been deposited to GEO accession number GSE227640 and can be accessed at https://www.ncbi.nlm.nih.gov/geo/query/acc.cgi?acc=GSE227640. Primary FACS-isolated oRG cells have been deposited to dbGAP

at accession number phs000989.v6.p1 and can be accessed at https://view.ncbi.nlm.nih.gov/dbgap-controlled. Details for data deposition are listed in the key resources table. No original code was written for this manuscript. Any additional information required to reanalyze the data reported in this paper is available from the lead contact upon request.

EXPERIMENTAL MODELS AND STUDY PARTICIPANT DETAILS

Pluripotent Stem Cell Lines—Previously described human PSC lines H1/WA01, H1/WA01 containing HOPX::citrine reporter, H28126, 13234 were used.[50,51] PSC lines were authenticated prior to differentiation. Every 10 passages, cells are tested for karyotypic abnormalities and validated for pluripotency markers Sox2, Nanog and Oct4. All cell lines tested negative for mycoplasma.

Pluripotent stem cell expansion culture—Human induced pluripotent stem cell lines, 13234 and H28126, and the embryonic stem cell line, WA01 (H1), were expanded on growth factor-reduced Matrigel-coated six well plates. Cells were thawed in StemFlex Pro (Gibco) media containing 10uM of Rock Inhibitor, Y-27632. Media was changed on alternate days where each line was passaged when wells reached ~70% confluency. Cells were passaged using ReLeSR (Stem Cell Technologies) and manual lifting, where residual cells were plated on fresh Matrigel-coated plates or frozen at −80C in mFresr (Stem cell technologies) for 24 hours before being moved to liquid nitrogen. All lines used in this study were between passage 20–40.

Cortical organoid differentiation protocol—Cortical organoids are differentiated using a regionalized forebrain differentiation protocol.[52,53] Stem cell lines were dissociated to single cells using accutase. After dissociation, cells were reconstituted in neural induction media maintaining a density of 10,000 cells per well of 96-well V-bottom ultra-low adhesion plates. Neural induction media is GMEM-based and includes 20% Knockout Serum Replacer (KSR), 1X non-essential amino acids, 0.11mg/mL Sodium Pyruvate, 1X Penicillin-Streptomycin, 0.1 mM Beta Mercaptoethanol, 5 μM SB431542 and 3 μM IWR1-endo. Cells were treated with 20 μM Rock inhibitor Y-27632 for the first 6 days. After 18 days, organoids were transferred to 6-well low adhesion plates and moved to an orbital shaker rotating at 90 RPM and transitioned into a DMEM/F12-based media containing 1X Glutamax, 1X N2, 1X CD Lipid Concentrate and 1X Penicillin-Streptomycin. After 35 days, organoids were moved into DMEM/F12-based media containing 10% FBS, 5ug/mL Heparin, 1X N2, 1X Chemically Defined Lipid Concentrate and 0.5% Matrigel. At 70 days media was additionally supplemented with 1X B27 and Matrigel concentration increased to 1%. Throughout culture duration organoids were fed every other day. For LIF treatment conditions, recombinant LIF protein (10 ng/ml, Millipore), SC144 (500 nM), or Ruxolitinib (1 μM) were mixed into organoid media. Organoids were treated with inhibitors beginning at 5 weeks of differentiation and with LIF protein either from weeks 6–8 or at week 5 onward.

Primary Cortical Tissue—All primary tissue samples were obtained and processed following approval 10–05113 by UCSF Gamete, Embryo and Stem Cell Research Committee (GESCR). Tissue was collected with consent from patients for research and

in strict observance of legal, institutional, and ethical regulations. All samples were de-identified and no sex information is known.

Organotypic slice culture of developing tissue—Primary cortical tissue from GW 19–23 was maintained in artificial cerebrospinal fluid (ACSF) containing 125 mM NaCl, 2.5 mM KCl, 1 mM MgCl2, 2 mM CaCl2, 1.25 mM NaH2PO4, 25 mM NaHCO3, and 25 mM D-(+)-glucose. Before use, ACSF was bubbled with 95% O2/5% CO2. Cortical tissue was embedded in a 3.5% low melt agarose gel. Embedded tissue was acutely sectioned at 300um using a vibratome (Leica) before being plated on Millicell (Millipore) inserts in 6 well tissue culture plates. Tissue slices were cultured at the air liquid interface in media containing 32% Hanks BSS, 60% BME, 5% FBS, 1% glucose, 1% N2 and 1% Penicillin-Streptomycin-Glutamine. Slices were maintained for 8 days in culture at 37°C and the media changed every other day. For LIF treatment conditions, recombinant LIF protein (10 ng/ml), SC144 (1 μM in slices), or Ruxolitinib (1 μM) were mixed into media prior to exposure to the tissue.

Cortical tissue dissociation—Primary cortical tissue was grossly minced using a scalpel. Small tissue pieces were then incubated in Papain (Worthington; #LK003178) resuspended in Earle's Balanced Salt Solution (EBSS) containing DNAse (Worthington; #LK003170) at 37°C for 30 – 45 mins. Tubes containing Papain solution and tissue were inverted every 10 mins to assist with the gentle tissue dissociation. After significant tissue dissociation, samples were then mechanically triturated to obtain a single cell suspension and centrifuged at 300g for 5 mins. The cell pellet was resuspended in dissociated cell culture medium (DMEM/F-12 Glutamax containing 1x B27, 1x N2, 1x Sodium Pyruvate and 1x Penicillin-Streptomycin), and filtered through 40μm nylon mesh cell strainers (fisherbrand). Dissociated cells were plated on poly-D-lysine and Matrigel-precoated plates.

METHOD DETAILS

Single cell capture and RNA sequencing—Organoids were dissociated with a Papain dissociation kit (Worthington) for 45 minutes, spun down at 300g for 5 min, resuspended in PBS + 0.5% BSA, filtered, and counted while verifying single cell dissociation. Single-cell capture was performed using 10X Genomics Chromium Single Cell 3' v2 kit per manufacturer's instructions. 10,000 cells were targeted for capture and 12 cycles of amplification for each of the cDNA amplification and library amplification were performed. Libraries were sequenced as per manufacturer recommendation on a NovaSeq S2 flow cell.

Primary oRGs immediately after FACS were directly subjected to cell counting and scRNAseq. oRGs and their progenies cultured in vitro for 4 weeks were first released by TrypLE Express (Gibco) before cell counting and scRNAseq. Single-cell capture was performed using 10X Genomics Chromium Single Cell 3' v3.1 kit per manufacturer's instructions, targeting 10,000 cells per reaction. Libraries were sequenced as per manufacturer recommendation on a NovaSeq S2 flow cell.

Organoid and tissue fixation and embedding—Organoids and organotypic slices were fixed in 4% PFA for 45 mins at 4°C, washed overnight at 4°C, and then incubated in

30% sucrose in 1X PBS overnight at 4°C. Once samples are saturated they will sink in the 30% sucrose solution. Samples were then embedded in cryomolds in a 3:2 solution mix of O.C.T. (Tissue-tek) and 30% sucrose in 1X PBS. Embedded samples were then frozen on dry ice and stored at −80°C. Frozen tissue was sectioned into thinly sectioned at 12μm using a cryostat (Leica) on glass slides and stored at −80°C. Dissociated cells were fixed in 4% PFA at RT for 10 minutes and washed with 1X PBS before immunostaining staining.

Fluorescence activated cell sorting (FACS)—Primary cortical tissue from GW15 – 19 was dissociated, as described above, and plated on poly-D-lysine and Matrigel precoated culture dishes in dissociated cell culture medium. 3–5 days after dissociation cells were released from plates using TrypLE (gibco, #12604–013) for 5–10 min. at 37°C. The cell suspension was spun down at 300g for 5 mins and resuspended in dissociation medium containing DNAse (1:100, Sigma-Aldrich, #D4513) and incubated at 37°C for 1 hr in low-binding plates or tubes to recover surface antigens. All subsequent steps were conducted on ice and all centrifugations at 4 °C. FACS buffer was prepared by adding DNAse and Y-27632 (1:1000) to 1% w/v Bovine serum albumin (BSA) in 2mM EDTA in D-PBS. Cells were spun down at 300g, washed 1x with FACS buffer, resuspended at 100 million cells per ml and incubated in FcR blocking reagent (1:20 in FACS buffer, Miltenyi Biotech, #130–059-901) for 10 mins. The conjugated antibody against LIFR (biotechne, #FAB249A) was added directly to the suspended cells (100 μl per 1 ml FACS buffer) and incubated for 30 minutes. Cells were washed in FACS buffer and resuspended for FACS according to pellet size. Cells were sorted using a BD FACSAria Flow Cytometer using unstained cells as a negative control for gating. Cells were sorted into FACS medium (20% v/v KSR, PS (1:100) and Rock inhibitor Y-27632 (10uM) in DMEM/F-12) and plated at 50,000 cells/well into pre-coated 8-chamber slides or 12 well plates. After 24 hours, the medium was switched to dissociation medium and LIF treatment was initiated. Media containing LIF recombinant protein (10 ng/ml) was changed every 2–3 days. Cells were cultured for one week with LIF treatment before being cultured for an additional three weeks without LIF. Controls were treated only with dissociation medium.

For lineage tracing experiments, primary cortical tissue from GW16 and 19 was processed as before with the following changes: individual LIFR+ cells were each sorted into a single well of 96-well glass-bottom plates pre-coated with matrigel containing 100 μl dissociation medium with FGF2 (10 ng/μl) using a BigFoot Spectral Cell Sorter (Thermo Fisher) via single-cell precision mode. Medium was changed to dissociation medium without any growth factor after one week and changed weekly for another 3 weeks. Cells were fixed and stained for immunohistochemistry 4 weeks after sorting.

Fluorescent *in situ* hybridization—Primary cortical tissue was cultured as organotypic slices before being fixed, embedded and sectioned, as described above. The RNAscope Multiplex Fluorescent Reagent Kit v2 (ACD Advanced Cell Diagnostics) and RNAscope probes against PCDH9 (Hs-PCDH9-C1; #1154001-C1), SCGN (Hs-SCGN-C2; #540331-C2), DLX5 (Hs-DLX5-C3; #569471-C3) and LIFR (Hs-LIFR, #441021) were used to detect RNA molecules in tissue. Fluorophores Opal-520 (1:500), Opal-570 (1:750) and Opal-690 (1:750) (all Akoya Biosciences) were used to detect the RNA probes. For sample

preparation, the slides with tissue sections were baked for 1 hr at 60°C, fixed in chilled 4% PFA for 15 mins at 4°C, submerged in boiling RNAscope target retrieval solution for 5 min., washed 2X with DI water and rinsed with 100% EtOH. Tissue sections were treated with RNAscope protease III for 30 minutes at 40°C and washed twice with DI water. RNAscope probes were hybridized for 2 hrs at 40°C and all subsequent steps were conducted according to the manufacturer's recommendation. As a negative control, untreated control and LIF-treated slices were incubated in TSA Buffer alone, without probes, during the probe incubation step. To ensure RNA integrity, RIN values of untreated controls and LIF-treated slices were measured. RNA was extracted from primary cortical tissue using the QIAGEN RNeasy Plus Micro Kit following the manufacturer's recommendation. RNA integrity was verified using an Agilent 2100 Bioanalyzer.

Immunohistochemistry—For organoids and primary tissue sections, antigen-retrieval was performed with 1x boiling citric acid-based antigen unmasking solution (Vector Laboratories) for 20 min. Slides were washed 1X with ddH2O and 3X with 1X PBS to remove the citrate solution. Tissue was blocked using a Donkey blocking buffer (DBB) containing 5% donkey serum, 2% gelatin and 0.1% Triton X-100 in 1X PBS (PBS-T) for >30 minutes at RT. Primary antibodies were incubated in DBB overnight at 4°C, washed 3X times with PBS-T, and incubated with AlexaFluor secondary antibodies (ThermoFisher and Jackson Labs) in DBB for 2 hrs at RT. Samples were washed 3X with PBS-T, 1X PBS, mounted, and dried overnight. Parallel sections were used as negative staining controls that were incubated in either primary or secondary, alone. Control slides were processed with antigen retrieval, washed with 1X PBS, and coverslipped like experimental samples. Negative controls were processed to ensure that fluorescence signal on experimental samples was not 'noise' from either autofluorescence or non-specific secondary binding. Images were acquired using a confocal white light microscope (Leica TCS SP5 X) where laser/gain settings were consistent upon acquisition of images from different samples within a single experiment.

QUANTIFICATION AND STATISTICAL ANALYSIS

Quantification and statistical analysis of immunohistochemistry—Total n are based on biological replicates where, whenever possible n=3 different biological individuals were analyzed. For organoids, the goal was to evaluate different stem cell lines across multiple (at least n=2) rounds of differentiation. Multiple organoids per PSC line/differentiation batch (n>2) were embedded within the same block and then serially sectioned where typically 10 total sections fit on one slide. For primary tissue, typically 2–3 sections were included on the same slide. Regardless of sample type, the entire slide was stained where different groups within an experiment were stained together with the same antibody process and mastermix. All sections on the slide are attempted to be imaged, where the organoid technical replicate and section are annotated. The individual data points on immunostaining graphs indicate the number of sections. For image capture, randomized, different areas of each organoid/tissue, per section were captured. All images, and cells within each captured image, were used for quantification. Cells counted for a given marker were normalized to Dapi to account for the organoid size.

For quantification of antibody and RNA probe abundance in organoids and tissue sections, the automated cell counter in the Imaris software (Bitplane) was used. All samples were normalized to sample area or number of DAPI+ nuclei. For experiments containing two conditions an unpaired two-tailed student's t-test or Mann-Whitney test, when not normally distributed, was used to analyze significant differences. For experiments with more than two conditions, a One-way ANOVA with multiple comparisons was used. Within an experiment, the control group was compared to each experimental group where significance determined according to: *p<0.05, **p<0.01, ***p<0.001, ****p<0.0001.

scRNAseq pre-processing and annotation—Cellranger (v2.0.0 for organoid samples and v7.0.2 for primary samples) from 10x Genomics was used for data pre-processing. Bcl files were converted to fastq using cellranger mkfastq. Barcode correction and reference genome alignment (GRCh38) were done using cellranger count with default parameters.

For organoid samples, count matrices were piped into Seurat v3,[54] in which cells with fewer than 500 genes or more than 10% of reads aligning to mitochondrial genes were discarded. Raw counts were log normalized with a size factor of 10,000 and clusters were identified using Louvain-Jaccard clustering. Clustering was performed using the Seurat package with a few modifications. Principal component analysis was performed using FastPCA, and significant principal components were identified.[55] In the space of these significant principal components, the k = 10 nearest neighbors were identified as per the RANN R package. The distances between these neighbors were weighted by their Jaccard distance, and Louvain clustering was performed using the igraph R package.[56] If any clusters contained only one cell, the process was repeated with k = 11 and upwards until no clusters contained only one cell.

For sorted or in vitro cultured primary human cortical samples, count matrices were piped into the R package Seurat v4[57] in which cells with fewer than 1000 genes, more than 10,000 genes, or more than 10% of reads aligning to mitochondrial genes were discarded. Raw counts were log normalized with a size factor of 10,000. The first 30 principal components were used to construct the k-nearest neighbors graph and Louvain clustering was used to identify clusters. Clusters with significantly fewer UMI counts, likely consisting of low-quality, dying cells, were also excluded for further analysis.

Cell type annotations of clusters were performed by comparison to previously annotated cell types,[20] and when a repository of substantial matching was not available, a combination of literature-based annotation of layer or maturation stage identity was used. UMAP embedding was computed for visualization.

Cluster-level correlation analysis for comparison across single-cell RNA sequencing datasets—Shi et al.[4] data were downloaded from GEO (GSE135827). The origins of cells (MGE, CGE, or LGE) were provided by the original authors in the metadata. We re-clustered the cells, annotated interneuron subtypes, and inferred the terminal cell types based on marker genes reported in the literature.[31] Uzquiano et al.[30] organoid data at 23 days, 3 months, and 6 months were downloaded from Single Cell Portal (SCP1756).

Raw counts from individual samples were normalized by SCTransform,[58] and cerebral organoid data were integrated with Shi et al.[4] data using the RPCA methods based on the top 3,000 most variable genes in the R package Seurat v4.[57] After integration, scaled gene matrices were extracted, and averaged expression levels of individual genes for each cell type/cluster were calculated. These resulting averaged gene expression profiles were used to calculate Spearman's rank correlation coefficients across datasets. Heatmaps were generated using the R package ComplexHeatmap (v2.8.0).[59]

Mutual nearest neighbors-based label transfer—As an alternative method to determine the identity of interneurons in organoid datasets, we performed mutual nearest neighbors-based label transfer using the MapQuery() function in Seurat v4. The first 30 principal components were used to identify transfer anchors. Labels from Shi et al.[4] were transferred to interneurons in organoid datasets when confidence was high (prediction score >0.5). Cells with prediction scores equal to or lower than 0.5 were labeled as unknown.

Eigengenes—Module eigengenes were calculated for numerous gene sets using the R package WGCNA.[60] Scores were generated for each set of up to 10,000 randomly subsetted cells from the group using the moduleEigengene function, Scores were calculated based on the intersection of the gene set of interest and genes expressed in the subset of cells. Eigenenes were defined as follows:

LGE genes: TSHZ1, PBX3, MEIS2, CALB2, CDCA7L, SYNPR, ETV1

CGE genes: SCGN, SP8, PCDH9, BTG1, NR2F1, NFIX, PROX1, NR2F2, SOX6, CXCR4

MGE genes: NKX2–1, LHX6, ACKR3, MAF, PDE1A, NXPH1

Supplementary Material

Refer to Web version on PubMed Central for supplementary material.

ACKNOWLEDGMENTS

The authors thank William Walantus, Maureen Galvez, and members of the A.R.K. and M.G.A. laboratories for useful discussions. This study was supported by NIH awards U01MH114825 and R35NS097305 to A.R.K. and R00MH125329 to M.G.A. Studies were funded through a Brain and Behavior Research Foundation NARSAD Young Investigator Grant #29155 to M.G.A. and the UCSF Program for Breakthrough Biomedical Research through the Sandler Foundation Faculty Fellows Program to G.P. Tissue collection was supported by the UCSF, the Neuropathology Core (Core B), and NINDS P01 grant (P01 NS083513). The graphical abstract was created using BioRender.com.

INCLUSION AND DIVERSITY

We support inclusive, diverse, and equitable conduct of research.

REFERENCES

1. Eze UC, Bhaduri A, Haeussler M, Nowakowski TJ, and Kriegstein AR (2021). Single-cell atlas of early human brain development highlights heterogeneity of human neuroepithelial cells and early radial glia. Nat. Neurosci 24, 584–594. 10.1038/s41593-020-00794-1. [PubMed: 33723434]

2. Bhaduri A, Sandoval-Espinosa C, Otero-Garcia M, Oh I, Yin R, Eze UC, Nowakowski TJ, and Kriegstein AR (2021). An atlas of cortical arealization identifies dynamic molecular signatures. Nature 598, 200–204. 10.1038/s41586-021-03910-8. [PubMed: 34616070]

3. Fan X, Fu Y, Zhou X, Sun L, Yang M, Wang M, Chen R, Wu Q, Yong J, Dong J, et al. (2020). Single-cell transcriptome analysis reveals cell lineage specification in temporal-spatial patterns in human cortical development. Sci. Adv 6, eaaz2978. 10.1126/sciadv.aaz2978.

4. Shi Y, Wang M, Mi D, Lu T, Wang B, Dong H, Zhong S, Chen Y, Sun L, Zhou X, et al. (2021). Mouse and human share conserved transcriptional programs for interneuron development. Science 374, eabj6641. 10.1126/science.abj6641.

5. Aldinger KA, Thomson Z, Phelps IG, Haldipur P, Deng M, Timms AE, Hirano M, Santpere G, Roco C, Rosenberg AB, et al. (2021). Spatial and cell type transcriptional landscape of human cerebellar development. Nat. Neurosci 24, 1163–1175. 10.1038/s41593-021-00872-y. [PubMed: 34140698]

6. Allaway KC, Gabitto MI, Wapinski O, Saldi G, Wang CY, Bandler RC, Wu SJ, Bonneau R, and Fishell G. (2021). Genetic and epigenetic coordination of cortical interneuron development. Nature 597, 693–697. 10.1038/s41586-021-03933-1. [PubMed: 34552240]

7. Ostrem B, Di Lullo E, and Kriegstein A. (2017). oRGs and mitotic somal translocation - a role in development and disease. Curr. Opin. Neurobiol 42, 61–67. 10.1016/j.conb.2016.11.007. [PubMed: 27978479]

8. Zimmer C, Tiveron MC, Bodmer R, and Cremer H. (2004). Dynamics of Cux2 expression suggests that an early pool of SVZ precursors is fated to become upper cortical layer neurons. Cereb. Cortex 14, 1408–1420. 10.1093/cercor/bhh102. [PubMed: 15238450]

9. Tarabykin V, Stoykova A, Usman N, and Gruss P. (2001). Cortical upper layer neurons derive from the subventricular zone as indicated by Svet1 gene expression. Development 128, 1983–1993. 10.1242/dev.128.11.1983. [PubMed: 11493521]

10. Lukaszewicz A, Savatier P, Cortay V, Giroud P, Huissoud C, Berland M, Kennedy H, and Dehay C. (2005). G1 phase regulation, area-specific cell cycle control, and cytoarchitectonics in the primate cortex. Neuron 47, 353–364. 10.1016/j.neuron.2005.06.032. [PubMed: 16055060]

11. Pollen AA, Nowakowski TJ, Chen J, Retallack H, Sandoval-Espinosa C, Nicholas CR, Shuga J, Liu SJ, Oldham MC, Diaz A, et al. (2015). Molecular identity of human outer radial glia during cortical development. Cell 163, 55–67. 10.1016/j.cell.2015.09.004. [PubMed: 26406371]

12. Nicola NA, and Babon JJ (2015). Leukemia inhibitory factor (LIF). Cytokine Growth Factor Rev. 26, 533–544. 10.1016/j.cytogfr.2015.07.001. [PubMed: 26187859]

13. Onishi K, and Zandstra PW (2015). LIF signaling in stem cells and development. Development 142, 2230–2236. 10.1242/dev.117598. [PubMed: 26130754]

14. Simamura E, Shimada H, Higashi N, Uchishiba M, Otani H, and Hatta T. (2010). Maternal leukemia inhibitory factor (LIF) promotes fetal neurogenesis via a LIF-ACTH-LIF signaling relay pathway. Endocrinology 151, 1853–1862. 10.1210/en.2009-0985. [PubMed: 20160138]

15. Hatta T, Moriyama K, Nakashima K, Taga T, and Otani H. (2002). The role of gp130 in cerebral cortical development: in vivo functional analysis in a mouse exo utero system. J. Neurosci 22, 5516–5524. 10.1523/JNEUROSCI.22-13-05516.2002. [PubMed: 12097503]

16. Bonaguidi MA, McGuire T, Hu M, Kan L, Samanta J, and Kessler JA (2005). LIF and BMP signaling generate separate and discrete types of GFAP-expressing cells. Development 132, 5503–5514. 10.1242/dev.02166. [PubMed: 16314487]

17. Watanabe M, Buth JE, Vishlaghi N, de la Torre-Ubieta L, Taxidis J, Khakh BS, Coppola G, Pearson CA, Yamauchi K, Gong D, et al. (2017). Self-organized cerebral organoids with human-specific features predict effective drugs to combat Zika virus infection. Cell Rep. 21, 517–532. 10.1016/j.celrep.2017.09.047. [PubMed: 29020636]

18. Dezonne RS, Sartore RC, Nascimento JM, Saia-Cereda VM, Romão LF, Alves-Leon SV, de Souza JM, Martins-de-Souza D, Rehen SK, and Gomes FCA (2017). Derivation of functional human astrocytes from cerebral organoids. Sci. Rep 7, 45091. 10.1038/srep45091. [PubMed: 28345587]

19. Nowakowski TJ, Bhaduri A, Pollen AA, Alvarado B, Mostajo-Radji MA, Di Lullo E, Haeussler M, Sandoval-Espinosa C, Liu SJ, Velmeshev D, et al. (2017). Spatiotemporal gene expression trajectories reveal developmental hierarchies of the human cortex. Science 358, 1318–1323. 10.1126/science.aap8809. [PubMed: 29217575]

20. Bhaduri A, Andrews MG, Mancia Leon W, Jung D, Shin D, Allen D, Jung D, Schmunk G, Haeussler M, Salma J, et al. (2020). Cell stress in cortical organoids impairs molecular subtype specification. Nature 578, 142–148. 10.1038/s41586-020-1962-0. [PubMed: 31996853]
21. Xu S, Oshima T, Imada T, Masuda M, Debnath B, Grande F, Garofalo A, and Neamati N. (2013). Stabilization of MDA-7/IL-24 for colon cancer therapy. Cancer Lett. 335, 421–430. 10.1016/j.canlet.2013.02.055. [PubMed: 23481022]
22. Pozios I, Hering NA, Guenzler E, Arndt M, Elezkurtaj S, Knösel T, Bruns CJ, Margonis GA, Beyer K, and Seeliger H. (2023). Gp130 is expressed in pancreatic cancer and can be targeted by the small inhibitor molecule SC144. J. Cancer Res. Clin. Oncol 149, 271–280. 10.1007/s00432-022-04518-9. [PubMed: 36495330]
23. Lin Q, Meloni D, Pan Y, Xia M, Rodgers J, Shepard S, Li M, Galya L, Metcalf B, Yue TY, et al. (2009). Enantioselective synthesis of Janus kinase inhibitor INCB018424 via an organocatalytic aza-Michael reaction. Org. Lett 11, 1999–2002. 10.1021/ol900350k. [PubMed: 19385672]
24. Gordon DE, Jang GM, Bouhaddou M, Xu J, Obernier K, White KM, O'Meara MJ, Rezelj VV, Guo JZ, Swaney DL, et al. (2020). A SARS-CoV-2 protein interaction map reveals targets for drug repurposing. Nature 583, 459–468. 10.1038/s41586-020-2286-9. [PubMed: 32353859]
25. Andrews MG, Subramanian L, and Kriegstein AR (2020). MTOR signaling regulates the morphology and migration of outer radial glia in developing human cortex. eLife 9. 10.7554/eLife.58737.
26. Trujillo CA, Gao R, Negraes PD, Gu J, Buchanan J, Preissl S, Wang A, Wu W, Haddad GG, Chaim IA, et al. (2019). Complex oscillatory waves emerging from cortical organoids model early human brain network development. Cell Stem Cell 25, 558–569.e7. 10.1016/j.stem.2019.08.002. [PubMed: 31474560]
27. Velasco S, Kedaigle AJ, Simmons SK, Nash A, Rocha M, Quadrato G, Paulsen B, Nguyen L, Adiconis X, Regev A, et al. (2019). Individual brain organoids reproducibly form cell diversity of the human cerebral cortex. Nature 570, 523–527. 10.1038/s41586-019-1289-x. [PubMed: 31168097]
28. Castro DS, Martynoga B, Parras C, Ramesh V, Pacary E, Johnston C, Drechsel D, Lebel-Potter M, Garcia LG, Hunt C, et al. (2011). A novel function of the proneural factor Ascl1 in progenitor proliferation identified by genome-wide characterization of its targets. Genes Dev. 25, 930–945. 10.1101/gad.627811. [PubMed: 21536733]
29. Delgado RN, Allen DE, Keefe MG, Mancia Leon WR, Ziffra RS, Crouch EE, Alvarez-Buylla A, and Nowakowski TJ (2022). Individual human cortical progenitors can produce excitatory and inhibitory neurons. Nature 601, 397–403. 10.1038/s41586-021-04230-7. [PubMed: 34912114]
30. Uzquiano A, Kedaigle AJ, Pigoni M, Paulsen B, Adiconis X, Kim K, Faits T, Nagaraja S, Antón-Bolaños N, Gerhardinger C, et al. (2022). Proper acquisition of cell class identity in organoids allows definition of fate specification programs of the human cerebral cortex. Cell 185, 3770–3788.e27. 10.1016/j.cell.2022.09.010. [PubMed: 36179669]
31. Schmitz MT, Sandoval K, Chen CP, Mostajo-Radji MA, Seeley WW, Nowakowski TJ, Ye CJ, Paredes MF, and Pollen AA (2022). The development and evolution of inhibitory neurons in primate cerebrum. Nature 603, 871–877. 10.1038/s41586-022-04510-w. [PubMed: 35322231]
32. Gelman DM, Marín O, and Rubenstein JLR (2012). The generation of cortical interneurons. In Jasper's Basic Mechanisms of the Epilepsies, Noebels JL, Avoli M, Rogawski MA, Olsen RW, and Delgado-Escuet AVa, eds. (National Center for Biotechnology Information).
33. Miyoshi G, Hjerling-Leffler J, Karayannis T, Sousa VH, Butt SJB, Battiste J, Johnson JE, Machold RP, and Fishell G. (2010). Genetic fate mapping reveals that the caudal ganglionic eminence produces a large and diverse population of superficial cortical interneurons. J. Neurosci 30, 1582–1594. 10.1523/JNEUROSCI.4515-09.2010. [PubMed: 20130169]
34. Hladnik A, Džaja D, Darmopil S, Jovanov-Milošević N, and Petanjek Z. (2014). Spatio-temporal extension in site of origin for cortical calretinin neurons in primates. Front. Neuroanat 8, 50. 10.3389/fnana.2014.00050. [PubMed: 25018702]
35. Condé F, Lund JS, Jacobowitz DM, Baimbridge KG, and Lewis DA (1994). Local circuit neurons immunoreactive for calretinin, calbindin D-28k or parvalbumin in monkey prefrontal cortex: distribution and morphology. J. Comp. Neurol 341, 95–116. 10.1002/cne.903410109. [PubMed: 8006226]

36. Gabbott PLA, Jays PRL, and Bacon SJ (1997). Calretinin neurons in human medial prefrontal cortex (areas 24a,b,c, 32′, and 25). J. Comp. Neurol 381, 389–410. 10.1002/(SICI)1096-9861(19970519)381:4<389::AID-CNE1>3.0.CO;2-Z. [PubMed: 9136798]
37. Fertuzinhos S, Krsnik Z, Kawasawa YI, Rasin MR, Kwan KY, Chen JG, Judas M, Hayashi M, and Sestan N. (2009). Selective depletion of molecularly defined cortical interneurons in human holoprosencephaly with severe striatal hypoplasia. Cereb. Cortex 19, 2196–2207. 10.1093/cercor/bhp009. [PubMed: 19234067]
38. Gordon A, Yoon SJ, Tran SS, Makinson CD, Park JY, Andersen J, Valencia AM, Horvath S, Xiao X, Huguenard JR, et al. (2021). Long-term maturation of human cortical organoids matches key early postnatal transitions. Nat. Neurosci 24, 331–342. 10.1038/s41593-021-00802-y. [PubMed: 33619405]
39. Molnár Z, Clowry GJ, Šestan N, Alzu'bi A, Bakken T, Hevner RF, Hüppi PS, Kostovic I, Rakic P, Anton ES, et al. (2019). New insights into the development of the human cerebral cortex. J. Anat 235, 432–451. 10.1111/joa.13055. [PubMed: 31373394]
40. Pașca SP, Arlotta P, Bateup HS, Camp JG, Cappello S, Gage FH, Knoblich JA, Kriegstein AR, Lancaster MA, Ming GL, et al. (2022). A nomenclature consensus for nervous system organoids and assembloids. Nature 609, 907–910. 10.1038/s41586-022-05219-6. [PubMed: 36171373]
41. Birey F, Andersen J, Makinson CD, Islam S, Wei W, Huber N, Fan HC, Metzler KRC, Panagiotakos G, Thom N, et al. (2017). Assembly of functionally integrated human forebrain spheroids. Nature 545, 54–59. 10.1038/nature22330. [PubMed: 28445465]
42. Bagley JA, Reumann D, Bian S, Lévi-Strauss J, and Knoblich JA (2017). Fused cerebral organoids model interactions between brain regions. Nat. Methods 14, 743–751. 10.1038/nmeth.4304. [PubMed: 28504681]
43. Samarasinghe RA, Miranda OA, Buth JE, Mitchell S, Ferando I, Watanabe M, Allison TF, Kurdian A, Fotion NN, Gandal MJ, et al. (2021). Identification of neural oscillations and epileptiform changes in human brain organoids. Nat. Neurosci 24, 1488–1500. 10.1038/s41593-021-00906-5. [PubMed: 34426698]
44. Santos GC, Silva DN, Fortuna V, Silveira BM, Orge ID, de Santana TA, Sampaio GL, Paredes BD, Ribeiro-Dos-Santos R, and Soares MBP (2020). Leukemia inhibitory factor (LIF) overexpression increases the angiogenic potential of bone marrow mesenchymal stem/stromal cells. Front. Cell Dev. Biol 8, 778. 10.3389/fcell.2020.00778. [PubMed: 32923442]
45. Winship A, Correia J, Krishnan T, Menkhorst E, Cuman C, Zhang JG, Nicola NA, and Dimitriadis E. (2015). Blocking endogenous leukemia inhibitory factor during placental development in mice leads to abnormal placentation and pregnancy loss. Sci. Rep 5, 13237. 10.1038/srep13237. [PubMed: 26272398]
46. Metcalfe SM (2011). LIF in the regulation of T-cell fate and as a potential therapeutic. Genes Immun. 12, 157–168. 10.1038/gene.2011.9. [PubMed: 21368774]
47. Warnier H, Barrea C, Bethlen S, Schrouff I, and Harvengt J. (2022). Clinical overview and outcome of the Stuve-Wiedemann syndrome: a systematic review. Orphanet J. Rare Dis 17, 174. 10.1186/s13023-022-02323-8. [PubMed: 35461249]
48. Dagoneau N, Scheffer D, Huber C, Al-Gazali LI, Di Rocco M, Godard A, Martinovic J, Raas-Rothschild A, Sigaudy S, Unger S, et al. (2004). Null leukemia inhibitory factor receptor (LIFR) mutations in Stuve-Wiedemann/Schwartz-Jampel type 2 syndrome. Am. J. Hum. Genet 74, 298–305. 10.1086/381715. [PubMed: 14740318]
49. Schneider CA, Rasband WS, and Eliceiri KW (2012). NIH Image to ImageJ: 25 years of image analysis. Nat. Methods 9, 671–675. 10.1038/nmeth.2089. [PubMed: 22930834]
50. Pollen AA, Bhaduri A, Andrews MG, Nowakowski TJ, Meyerson OS, Mostajo-Radji MA, Di Lullo E, Alvarado B, Bedolli M, Dougherty ML, et al. (2019). Establishing cerebral organoids as models of human-specific brain evolution. Cell 176, 743–756.e17. 10.1016/j.cell.2019.01.017. [PubMed: 30735633]
51. Edel MJ (2018). iPS Cells for Modelling and Treatment of Human Diseases (MDPI).
52. Kadoshima T, Sakaguchi H, Nakano T, Soen M, Ando S, Eiraku M, and Sasai Y. (2013). Self-organization of axial polarity, inside-out layer pattern, and species-specific progenitor dynamics

in human ES cell-derived neocortex. Proc. Natl. Acad. Sci. USA 110, 20284–20289. 10.1073/pnas.1315710110. [PubMed: 24277810]

53. Bershteyn M, Nowakowski TJ, Pollen AA, Di Lullo E, Nene A, Wynshaw-Boris A, and Kriegstein AR (2017). Human iPSC-derived cerebral organoids model cellular features of lissencephaly and reveal prolonged mitosis of outer radial glia. Cell Stem Cell 20, 435–449.e4. 10.1016/j.stem.2016.12.007. [PubMed: 28111201]
54. Stuart T, Butler A, Hoffman P, Hafemeister C, Papalexi E, Mauck WM, Hao Y, Stoeckius M, Smibert P, and Satija R. (2019). Comprehensive Integration of Single-Cell Data. Cell 177, 1888–1902.e21. 10.1016/j.cell.2019.05.031. [PubMed: 31178118]
55. Nowakowski TJ, Bhaduri A, Pollen AA, Alvarado B, Mostajo-Radji MA, Di Lullo E, Haeussler M, Sandoval-Espinosa C, Liu SJ, Velmeshev D, et al. (2017). Spatiotemporal gene expression trajectories reveal developmental hierarchies of the human cortex. Science 358, 1318–1323. 10.1126/science.aap8809. [PubMed: 29217575]
56. Csardi G, and Nepusz T. (2006). The igraph software package for complex network research (InterJournal Complex Systems).
57. Hao Y, Hao S, Andersen-Nissen E, Mauck WM 3rd, Zheng S, Butler A, Lee MJ, Wilk AJ, Darby C, Zager M, et al. (2021). Integrated analysis of multimodal single-cell data. Cell 184, 3573–3587.e29. 10.1016/j.cell.2021.04.048. [PubMed: 34062119]
58. Hafemeister C, and Satija R. (2019). Normalization and variance stabilization of single-cell RNA-seq data using regularized negative binomial regression. Genome Biol. 20, 296. 10.1186/s13059-019-1874-1. [PubMed: 31870423]
59. Gu Z, Eils R, and Schlesner M. (2016). Complex heatmaps reveal patterns and correlations in multidimensional genomic data. Bioinformatics 32, 2847–2849. 10.1093/bioinformatics/btw313. [PubMed: 27207943]
60. Langfelder P, and Horvath S. (2008). WGCNA: an R package for weighted correlation network analysis. BMC Bioinformatics 9, 559. 10.1186/1471-2105-9-559. [PubMed: 19114008]

Highlights

- Outer radial glia proliferation and differentiation are regulated by LIF signaling
- LIF exposure promotes interneuron differentiation in cortical cultures
- Interneurons in forebrain organoids resemble caudal ganglionic eminence cells
- Isolated outer radial glia can produce interneurons, which LIF treatment increases

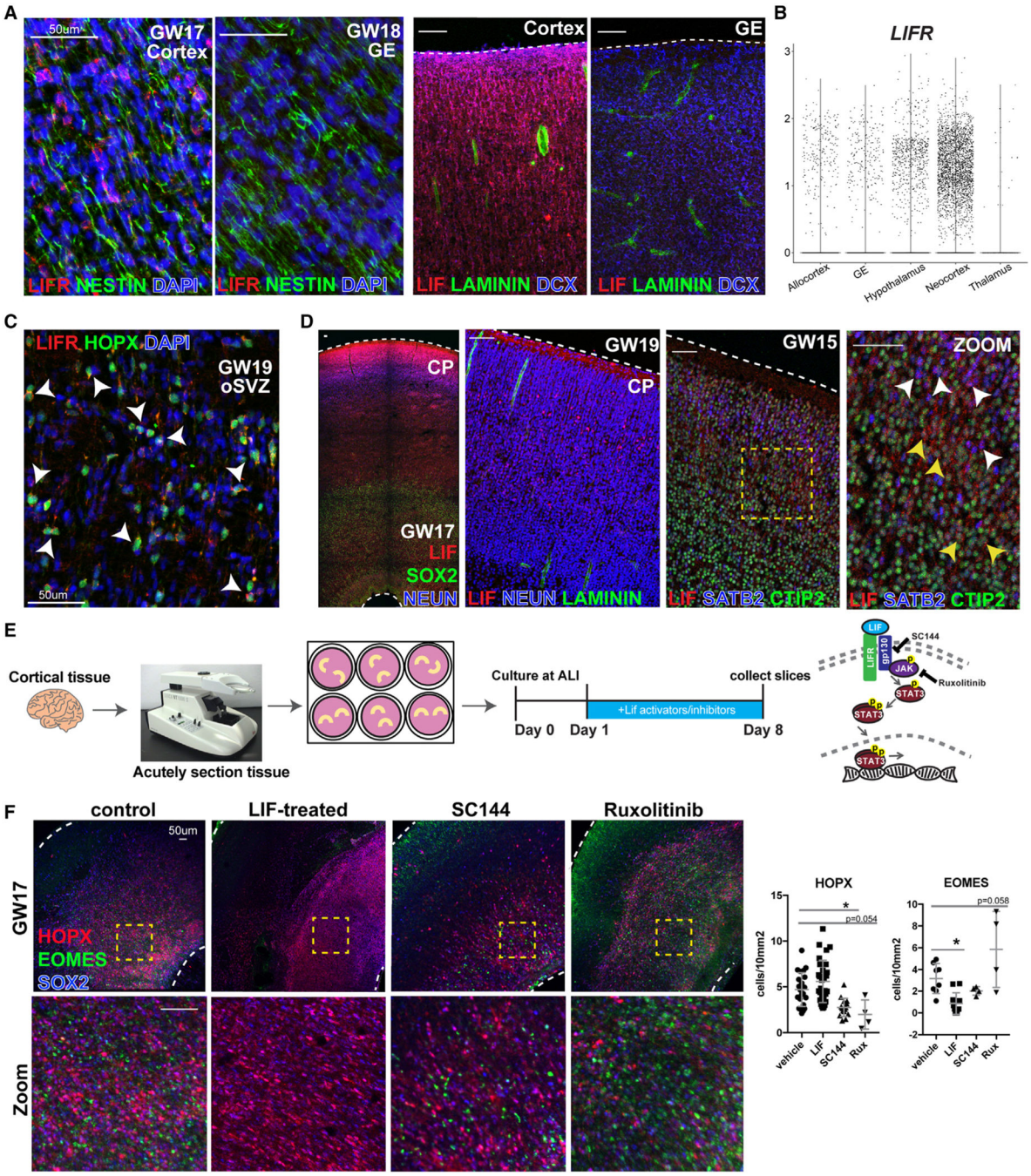

Figure 1. LIF signaling mediators are present in the dorsal, but not in the ventral, cortex, and LIF signaling perturbation impacts the ratio of oRGs and IPCs in cortical tissue

(A) During GW17 and GW18, LIFR is present in the oSVZ on NESTIN+ RG in the dorsal neocortex, but not in the ventral GE. LIF co-labels DCX+ neurons in the CP, but not in the GE. LAMININ+ vascular cells are in both cortex and GE.

(B) Reanalysis of human neural tissue[2] identified highest *LIFR* expression in the neocortex.

(C) LIFR is present in HOPX+ oRG cells in the oSVZ (white arrowheads) of GW19 cortical tissue.

(D) LIF expression overlaps with NEUN+ excitatory neurons that are CTIP2+ (yellow arrowheads) or SATB2+ (white arrowheads) during GW15–19.
(E) Cortical tissue was sliced, cultured at air liquid interface (ALI), and treated with LIF, SC144, or ruxolitinib for 1 week.
(F) LIF inhibition decreases HOPX+ oRG cells, whereas LIF addition reduces EOMES+ IPCs (one-way ANOVA with multiple comparisons, HOPX: vehicle vs. SC144: *$p < 0.018$, vehicle vs. Rux: $p = 0.0539$; EOMES: vehicle vs. LIF: *$p < 0.0252$, vehicle vs. SC144: $p = 0.6552$, vehicle vs. Rux: $p = 0.0576$, $n = 7$ biological samples). Data are represented as mean ± SD.

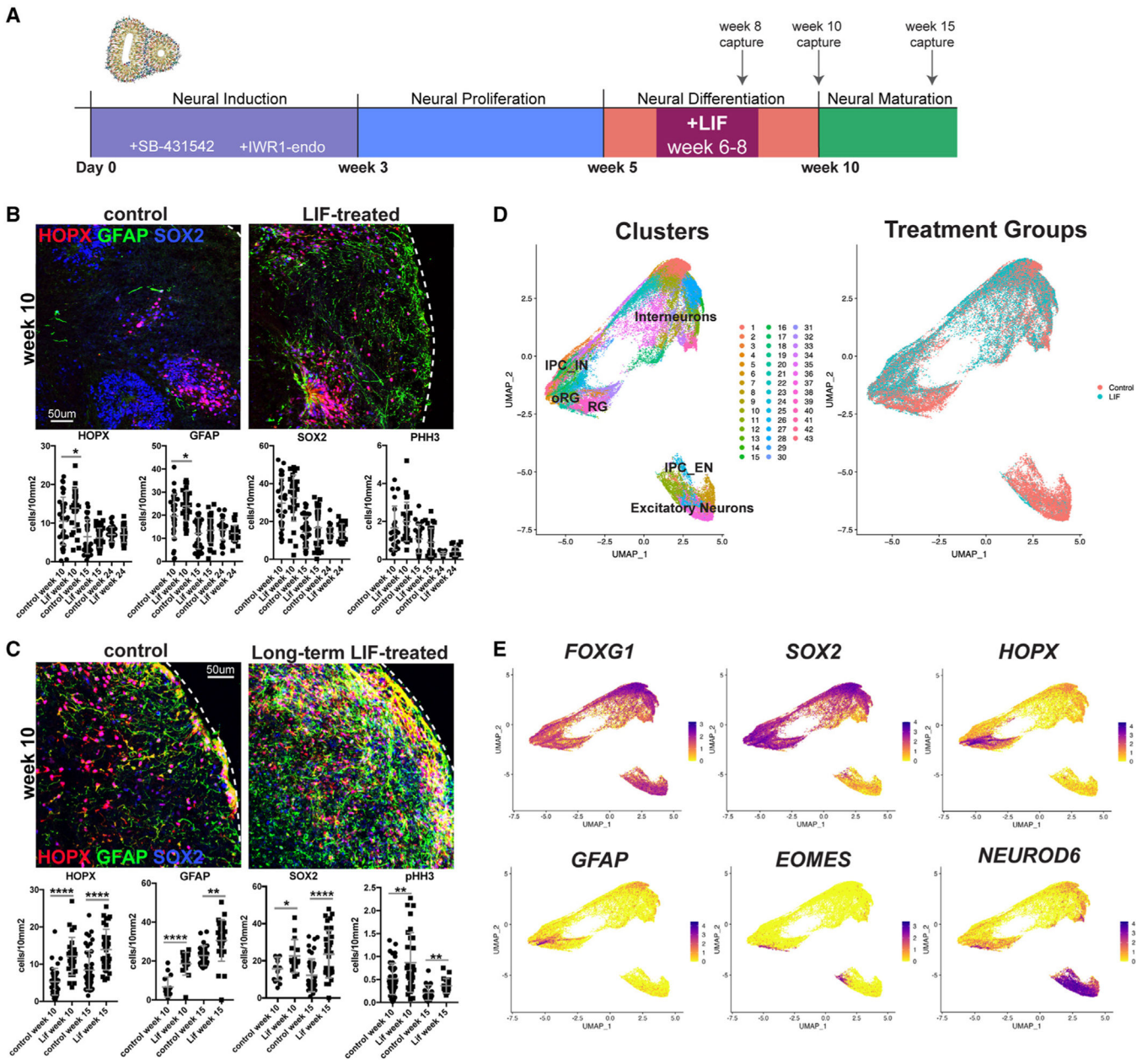

Figure 2. LIF signaling increases the number of oRG cells in forebrain organoids

(A) Protocol for dorsal forebrain organoid induction.

(B) LIF treatment during weeks 6–8 increases the number of HOPX+ (unpaired t test: week 10: *p = 0.024, n = 5 differentiation batches from 3 lines) and GFAP+ (unpaired t test: *p < 0.04, n = 5 batches from 3 lines) oRG cells in week 10 organoids. No changes in SOX2+ or pHH3+ cells were observed (unpaired student t tests; p > 0.05 for all comparisons). Data are represented as mean ± SD.

(C) Continuous LIF treatment increases SOX2+ (unpaired t test for control vs. LIF, week 10: *p < 0.0185, n = 3 batches from 3 lines; week 15: ****p < 0.0001,n = 4 batches from 3 lines), pHH3+ (unpaired t test, week 10: **p < 0.0034, n = 5 batches from 3 lines, week 15: **p < 0.0054, n = 2 batches from 2 lines), HOPX+ (unpaired t test: week 10: ****p <

0.0001, n = 5 batches from 3 lines; week 15: ****p < 0.0001, n = 3 batches from 3 lines) and GFAP+ oRG cells (unpaired t test, week 10: ****p < 0.0001, n = 3 batches from 3 lines; week 15: **p < 0.0018, n = 2 batches from 2 lines). Data are represented as mean ± SD.
(D) Uniform Manifold Approximation and Projection (UMAP) plots separated by cluster and treatment group.
(E) Feature plots showing the expression of cortical markers *FOXG1*, *SOX2*, *HOPX*, *GFAP*, *EOMES*, and *NEUROD6*.

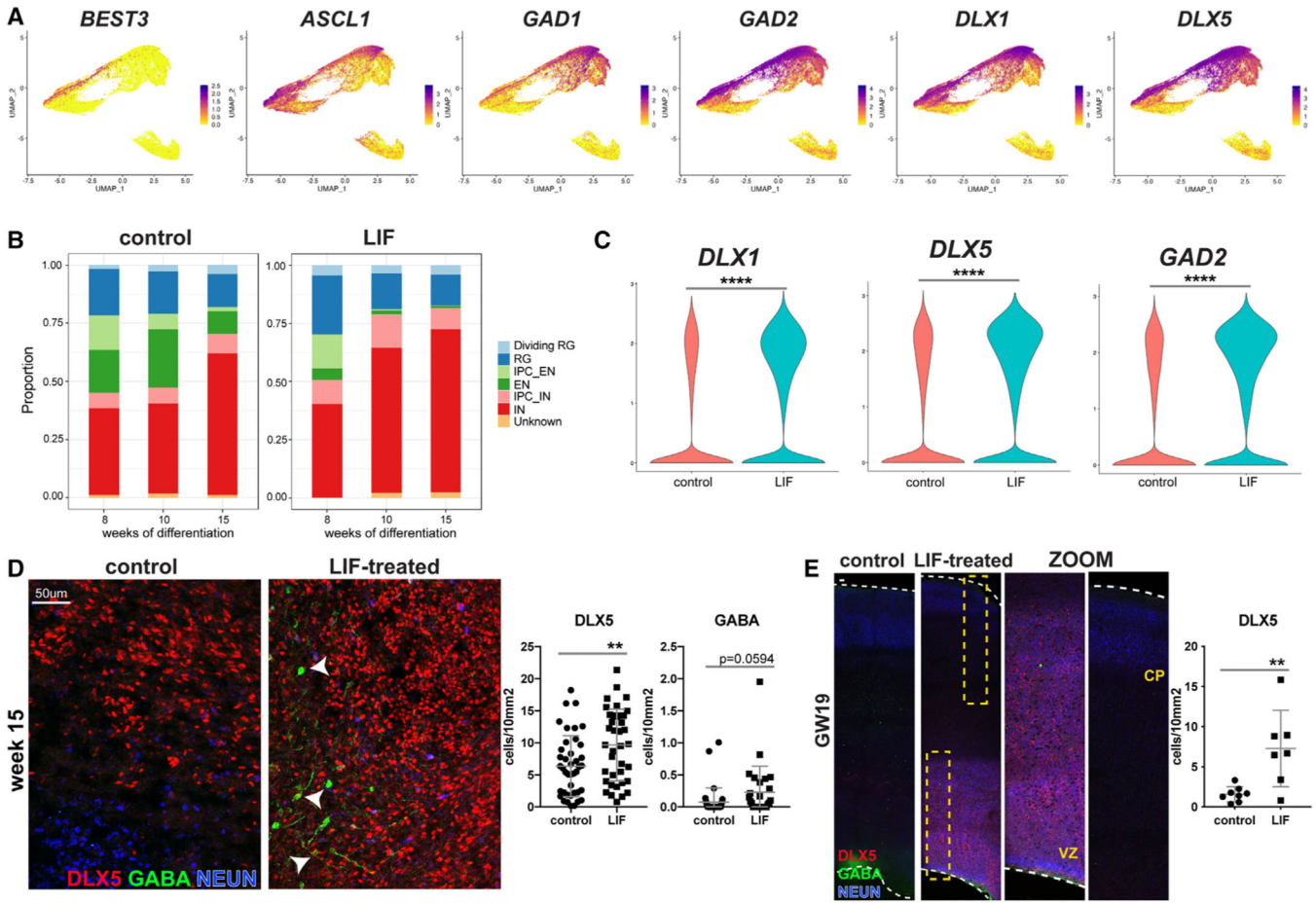

Figure 3. DLX+ IN-like cells are present in forebrain organoids and cortical tissue and increase after LIF treatment

(A) Feature plots of IN_IPC markers, *ASCL1* and *BEST3*, and IN markers, *GAD1*, *GAD2*, *DLX1*, and *DLX5* in weeks 8–15 organoids.

(B) Proportions of cell types in organoids captured in scRNA-seq.

(C) Violin plots of IN markers (*DLX1*: ****p < 7.58×10^{-56}, *DLX5*: ****p < 4.04×10^{-48}, *GAD2*: ****p < 2.2×10^{-52}) in organoids with and without LIF treatment between weeks 6 and 8.

(D) Quantification of DLX5+ (unpaired t test, **p < 0.0059, n = 3 differentiation batches across 3 lines) and GABA+ (unpaired t test, p = 0.0594, n = 2 batches across 2 lines) cells (white arrowheads). Data are represented as mean ± SD.

(E) Quantification of DLX5+ cells in organotypic slice cultures of GW15–19 cortical tissue (unpaired t test, **p < 0.0054, n = 6 biological samples from GW18 to GW19). Data are represented as mean ± SD.

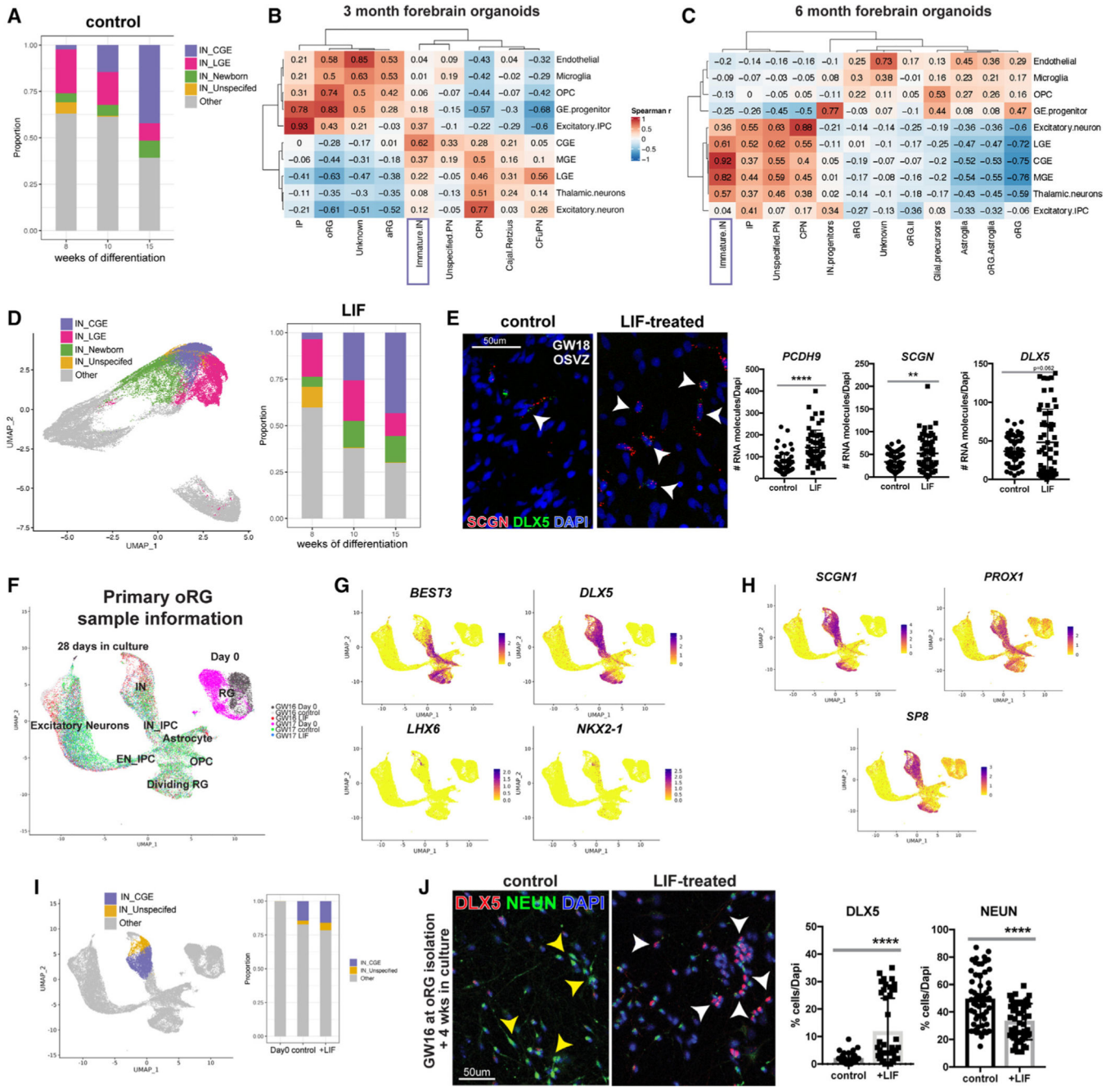

Figure 4. CGE-like INs are present in dorsal forebrain organoids and oRG-derived cultures and increase after LIF treatment

(A) Proportions of IN subtypes in forebrain organoids captured in scRNA-seq.

(B) Correlations between 3 month organoid[30] and primary GE datasets.[4]

(C) Correlations between 6 month organoids[30] and primary GE datasets.[4]

(D) UMAP of IN subtypes and proportions in organoids treated with LIF during peak oRG expansion.

(E) *In situ* hybridization of *PCDH9* (unpaired t test, ****p < 0.0001, n = 3 biological samples), *SCGN* (unpaired t test, **p < 0.0014, n = 3 biological samples), and *DLX5*

(unpaired t test, p = 0.0624, n = 3 biological samples) in the oSVZ of GW18 and GW19 cortical slices treated with and without LIF (white arrowheads). Data are represented as mean ± SD.

(F) UMAP of FACS-isolated RGs at day 0 and progeny after 4 weeks in culture.

(G) Feature plots of IPC_IN marker *BEST3*+, IN marker *DLX5*+, and MGE markers *LHX6* and *NKX2–1*.

(H) Feature plots of CGE markers *SCGN*, *PROX1*, and *SP8*.

(I) Proportions of IN subtypes derived from FACS-isolated oRG cells captured in scRNA-seq.

(J) GW16 FACS-isolated oRG cells cultured under control and LIF-treated conditions (DLX5: ****p < 0.0001; NEUN ****p < 0.0001, n = 4 biological samples). Data are represented as mean ± SD.

KEY RESOURCES TABLE

REAGENT or RESOURCE	SOURCE	IDENTIFIER
Antibodies		
anti-CTIP2, rat, 1:500	Abcam	Cat#ab18465 RRID: AB_2064130
anti-DLX5, rabbit, 1:100	Sigma	Cat#HPA005670 RRID:AB_1078681
anti-EOMES, sheep, 1:250	R&D Systems	Cat#AF6166 RRID: AB_10569705
anti-GFAP, goat, 1:500	Abcam	Cat#ab4674 RRID:AB_304558
anti-GFP, chicken, 1:500	Aves labs	Cat#GFP-1020 RRID: AB_300798
anti-HOPX, rabbit, 1:250	Proteintech	Cat#11419-1-AP RRID:AB_10693525
anti-LIF, rabbit, 1:100	Proteintech	Cat#26757-1-AP RRID:AB_2880624
anti-LIFR, rabbit, 1:50	Abcam	Cat#235908 RRID: NA
anti-LIFR-APC conjugated, mouse, 1:10	Biotechne	Cat#FAB249A RRID:NA
anti-NEUN, guinea pig, 1:500	Millipore	Cat#ABN90 RRID: AB_11205592
anti-NR2F2, mouse, 1:250	Perseus proteomics	Cat#PP-H7147-00 RRID:AB_1964214
anti-PAX6, rabbit, 1:500	Biolegend	Cat#901301 RRID:AB_2565003
anti-pHH3, mouse, 1:500	Abcam	Cat#ab14955 RRID:AB_443110
anti-SATB2, mouse, 1:500	Abcam	Cat#ab51502 RRID: AB_882455
anti-SCGN, rabbit, 1:250	Sigma	Cat#HPA006641 RRID:AB_1079874
anti-SOX2, mouse, 1:500	Santa Cruz	Cat#Sc-365823 RRID:AB_10842165
anti-VIM, chicken, 1:500	Millipore	Cat#ab5733 RRID:AB_11212377
Chemicals, peptides, and recombinant proteins		
Rock Inhibitor Y-27632, 10 uM or 20 uM	Stemcell Technologies	Cat# 72304
IWR-1-endo, 3 uM	Cayman Chemical	Cat# 13659
SB43152, 5 uM	Tocris	Cat# 1614
Recombinant LIF protein, 10 ng/ml	Millipore	Cat# LIF1010
FGF2, 10 ng/ml	Gibco	Cat# PHG0369
SC144, 1 um	Selleck Chemicals	Cat# S7124
Ruxolitinib, 1 uM	Selleck Chemicals	Cat# S13783
Critical commercial assays		
Chromium Single Cell 3’ v3.1 kit	10x Genomics	Cat# PN-1000121
RNAscope Multiplex Fluorescent Reagent Kit v2	ACD Advanced Cell Diagnostics	Cat# 323100
Worthington Dissociation kit	Worthington Biochemical	LK003153
Deposited data		
Raw and processed Lif organoid data	this paper	GEO: GSE227640
Raw and processed primary tissue data	this paper	dbGAP: phs000989.v6.p1
Experimental models: Cell lines		
H1/WA01 human embryonic stem cell line, male	WiCell Research Institute	RRID: CVCL_9771

REAGENT or RESOURCE	SOURCE	IDENTIFIER
H1/WA01 human embryonic stem cell line containing HOPX::citrine reporter	Allen Institute - Dr. Boaz Levi	NIH: NIHhESC-10-0043
H28126 human induced pluripotent stem cell line, male	Gilad-26102527	RRID: NA
13234 human induced pluripotent stem cell line, female	Conklin lab	RRID: CVCL_0G84
Primary cortical tissue samples (GW15-19)	UCSF GESCR committee	De-identified
Oligonucleotides (RNAscope probes)		
Hs-PCDH9-C1	ACD Advanced Cell Diagnostics	Cat#1154001-C1
Hs-SCGN-C2	ACD Advanced Cell Diagnostics	Cat#540331-C2
Hs-DLX5-C3	ACD Advanced Cell Diagnostics	Cat#569471-C3
Hs-LIFR	ACD Advanced Cell Diagnostics	Cat#441021
Software and algorithms		
Fiji	Schneider et al.[49]	RRID: SCR_002285
Imaris	Oxford Instruments	RRID: SCR_007370
Prism	GraphPad Prism Version 10.6.2	RRID: SCR_002798
Flowjo	FlowJo Version 10.6.2	RRID: SCR_008520
R	The R foundation	RRID: SCR_001905
Adobe Illustrator	Adobe	RRID: SCR_010279